

September 2019 Antarctic sudden stratospheric warming: quasi-6-day wave burst and ionospheric effects

Yosuke Yamazaki¹, Vivien Matthias², Yasunobu Miyoshi³, Claudia Stolle⁴, Tarique Siddiqui⁴, Guram Kervalishvili⁵, Jan Lastovička⁶, Michal Kozubek⁷, William Edmund Ward⁸, David R. Themens⁸, Samuel Kristoffersen⁸, and Patrick Alken⁹

¹GFZ German Research Centre for Geosciences

²Potsdam Institute for Climate Impact Research

³Kyushu University

⁴GFZ Potsdam

⁵Helmholtz Centre Potsdam-GFZ, German Research Center for Geosciences

⁶Institute of Atmospheric Physics of the Czech Academy of Sciences, Bocni II, 14131 Prague 4, Czech Republic

⁷Institute of Atmospheric Physics CAS

⁸University of New Brunswick

⁹University of Colorado Boulder

November 21, 2022

Abstract

An exceptionally strong stationary planetary wave with Zonal Wavenumber 1 led to a sudden stratospheric warming (SSW) in the Southern Hemisphere in September 2019. Ionospheric data from ESA's Swarm satellite constellation mission reveal prominent 6-day variations in the dayside low-latitude region at this time, which can be attributed to forcing from the middle atmosphere by the Rossby normal mode "quasi-6-day wave" (Q6DW). Geopotential height measurements by the Microwave Limb Sounder aboard NASA's Aura satellite show a burst of Q6DW activity in the mesosphere and lower thermosphere during the SSW, which is one of the strongest in the record. The Q6DW is apparently generated in the polar stratosphere at 30-40 km, where the atmosphere is unstable due to strong vertical wind shear connected with planetary-wave breaking. These results suggest that an Antarctic SSW can lead to ionospheric variability through wave forcing from the middle atmosphere.

22 **Abstract**

23 An exceptionally strong stationary planetary wave with Zonal Wavenumber 1 led
24 to a sudden stratospheric warming (SSW) in the Southern Hemisphere in September 2019.
25 Ionospheric data from ESA’s Swarm satellite constellation mission reveal prominent 6-
26 day variations in the dayside low-latitude region at this time, which can be attributed
27 to forcing from the middle atmosphere by the Rossby normal mode “quasi-6-day wave”
28 (Q6DW). Geopotential height measurements by the Microwave Limb Sounder aboard
29 NASA’s Aura satellite show a burst of Q6DW activity in the mesosphere and lower ther-
30 mosphere during the SSW, which is one of the strongest in the record. The Q6DW is
31 apparently generated in the polar stratosphere at 30–40 km, where the atmosphere is
32 unstable due to strong vertical wind shear connected with planetary-wave breaking. These
33 results suggest that an Antarctic SSW can lead to ionospheric variability through wave
34 forcing from the middle atmosphere.

1 Introduction

A sudden stratospheric warming (SSW) is a large-scale meteorological phenomenon in the winter stratosphere, which involves a rapid rise in the polar temperature by a few tens of K in several days (Andrews, Leovy, & Holton, 1987; Labitzke & Van Loon, 1999). An SSW is triggered by an injection of stationary planetary waves (PWs) from the troposphere, which are driven by topography and land-sea temperature contrasts. PW breaking in the middle atmosphere leads to an acceleration of the zonal mean flow and changes the mean meridional circulation (Matsuno, 1971). Dynamical effects of PW breaking during SSWs are not limited in the stratosphere but are also well extended into the mesosphere and lower thermosphere (Chandran, Collins, & Harvey, 2014).

According to the definition by the World Meteorological Organization (McInturff, 1978), a “minor” SSW occurs when a large temperature increase is observed in the winter polar stratosphere, at least by 25 K in a week or less. The event is called “major” if the reversal of the zonal mean flow from eastward to westward occurs poleward of 60° latitude at 10 hPa (32 km) or below, along with the reversal of the meridional temperature gradient. The average number of major SSWs is ~ 0.6 per winter in the Northern Hemisphere (NH) (Butler et al., 2015; Charlton & Polvani, 2007). In the Southern Hemisphere (SH), the occurrence of an SSW, whether major or minor, is not as frequent as in the NH because of weaker PW forcing due to smaller topographical differences and land-sea contrasts. In fact, the September 2002 event (Baldwin, Hirooka, O’Neill, & Yoden, 2003; Krüger, Naujokat, & Labitzke, 2005) is the only major SSW observed in the Antarctic.

In the last decade, the aeronomy community has come to the realization that SSWs can be a significant source of ionospheric variability (Chau, Goncharenko, Fejer, & Liu, 2012; Pedatella et al., 2018). In particular, the January 2009 major Arctic SSW, which took place under extremely quiet solar- and geomagnetic-activity conditions, enabled many studies to attribute observed ionospheric perturbations to the SSW (e.g., Chau et al., 2010; Fejer et al., 2010; Goncharenko, Chau, Liu, & Coster, 2010; Goncharenko, Coster, Chau, & Valladares, 2010; Lin et al., 2019; H. Liu et al., 2011; Nayak & Yiğit, 2019; Oyama et al., 2014; Pancheva & Mukhtarov, 2011; Patra, Pavan Chaitanya, Sripathi, & Alex, 2014; Pedatella & Forbes, 2010; Rodrigues, Crowley, Azeem, & Heelis, 2011; Yadav et al., 2017; Yue et al., 2010). Most studies concentrated on the dayside low-latitude re-

67 gion, where the ionospheric response to the SSW was most pronounced. Modeling stud-
68 ies have suggested that atmospheric tides played an important role in driving ionospheric
69 variability during the January 2009 SSW (Fang et al., 2012; Fuller-Rowell et al., 2011;
70 Jin et al., 2012; Pedatella et al., 2014; Pedatella & Maute, 2015; Sassi, Liu, Ma, & Gar-
71 cia, 2013; Wang et al., 2014). Tidal waves at altitudes of the ionospheric E region (95–
72 150 km) are, in large part, from the middle atmosphere, and their amplitudes and phases
73 can change in response to an SSW (Stening, Forbes, Hagan, & Richmond, 1997). Among
74 different tidal modes, the semidiurnal lunar tide shows a particularly strong and con-
75 sistent response to SSWs (Chau, Hoffmann, Pedatella, Matthias, & Stober, 2015; Zhang
76 & Forbes, 2014). Forbes and Zhang (2012) argued that the large semidiurnal lunar tide
77 observed during the January 2009 SSW can arise from resonant amplification associated
78 with the atmospheric Pekeris mode. Enhanced lunar tidal perturbations in the equato-
79 rial ionosphere have been reported for a number of SSW events (Fejer, Tracy, Olson, &
80 Chau, 2011; J. Liu, Zhang, Hao, & Xiao, 2019; Park, Lühr, Kunze, Fejer, & Min, 2012;
81 Siddiqui et al., 2018; Siddiqui, Stolle, Lühr, & Matzka, 2015; Yamazaki, Richmond, &
82 Yumoto, 2012).

83 As mentioned earlier, SSWs rarely occur in the SH, and the ionospheric response
84 to Antarctic SSWs has been largely unexplored. The only exception is the study by Ol-
85 son, Fejer, Stolle, Lühr, and Chau (2013), which examined ionospheric variability dur-
86 ing the September 2002 major Antarctic SSW. Although Olson et al. (2013) observed
87 multi-day variations in the equatorial ionosphere, their association with the SSW remained
88 somewhat uncertain because of high geomagnetic activity during the event. The main
89 objective of this study is to present observations from the ionosphere and middle atmo-
90 sphere during the recent Antarctic SSW event in September 2019 and note the presence
91 of unusually strong traveling PW activity throughout the atmosphere and ionosphere
92 at this time.

93 **2 Results and Discussion**

94 **2.1 September 2019 sudden stratospheric warming**

95 Figure 1 gives an overview of the September 2019 SSW. The polar temperature at
96 10 hPa, obtained from the MERRA-2 reanalysis (Gelaro et al., 2017), shows a rapid in-
97 crease from 207.7 K on 5 September to 258.5 K on 11 September 2019 ($\Delta T=50.8$ K/week)

98 (Figure 1a). This is the largest increase in the Antarctic polar temperature per week in
99 the entire MERRA-2 data set starting from January 1980. The maximum temperature
100 rise during the September 2002 major SSW was $\Delta T=38.5$ K/week. Figure 1b presents
101 the vertical structure of the zonal mean zonal wind at 60°S, as derived from geopotential
102 height (GPH) measurements by the Aura Microwave Limb Sounder (MLS) (Schwartz
103 et al., 2008; Waters et al., 2006). It can be seen that the eastward zonal mean wind first
104 reversed in the upper mesosphere on 2 September 2019, and in the subsequent days, the
105 region of the wind reversal descended to lower layers, reaching 40 km on 18 September
106 2019. Since the wind reversal did not reach the 10 hPa level (~ 32 km), the event is cat-
107 egorized as a minor warming. Figure 1c shows that there was an enhancement in the am-
108 plitude of the stationary PW with Zonal Wavenumber (ZW) 1 during 14–20 August 2019
109 and during 28 August–5 September 2019. In both cases, the amplitude attained the largest
110 recorded by Aura/MLS since August 2004. The former event can contribute to the SSW
111 by weakening the zonal mean flow, which is often referred to as preconditioning (e.g.,
112 Cámara et al., 2017; Limpasuvan, Thompson, & Hartmann, 2004; McIntyre, 1982). Forc-
113 ing due to PW breaking during the latter event is the likely cause of the zonal wind re-
114 versal in the middle atmosphere, and hence the SSW. No similar enhancement is found
115 in the amplitude of the stationary PW with ZW2.

116 As a brief summary, the September 2019 Antarctic SSW was a minor warming but
117 it involved an exceptionally strong stationary PW with ZW1 and a large temperature
118 rise. Furthermore, the event took place during the minimum phase of the solar cycle, sim-
119 ilar to the January 2009 SSW, and as will be shown later, overall solar and geomagnetic
120 activities were low, which helps identify SSW effects on the ionosphere. Therefore, the
121 September 2019 event provides an excellent (and rare) opportunity to investigate the iono-
122 spheric response to an Antarctic SSW, which is not well understood from previous stud-
123 ies.

124 **2.2 Ionospheric observations by Swarm**

125 ESA’s Earth observation mission Swarm (Friis-Christensen, Lühr, & Hulot, 2006)
126 involves three identical satellites (A, B and C), equipped with scientific instruments that
127 are suitable for investigating Earth’s magnetic field and its source currents (Friis-Christensen,
128 Lühr, Knudsen, & Haagmans, 2008). The three spacecraft were launched into polar or-
129 bits on 22 November 2013, and since 17 April 2014, Swarm A and C fly side-by-side at

130 an altitude of ~ 460 km while Swarm B flies at ~ 510 km. Figures 2a–2c show the tem-
131 poral variability of the equatorial electrojet (EEJ) intensity (e.g., Alken et al., 2015), elec-
132 tron density (e.g., Buchert et al., 2015), and total electron content (TEC) (e.g., Park et
133 al., 2017) as observed by Swarm B during 5 September–5 October 2019. The data used
134 here were collected from the descending parts of the orbit in 11:00–14:00 magnetic lo-
135 cal time (MLT) (see also Figure 2g). Figures 2h and 2i show that overall solar and ge-
136 omagnetic activity levels were low during this time interval, which is typical for solar min-
137 imum conditions. Moderately high geomagnetic activity was observed during 27 September–
138 1 October 2019, which needs to be taken into account when the ionospheric data are in-
139 terpreted. Unlike the September 2002 Antarctic SSW, which was examined by Olson et
140 al. (2013), severe geomagnetic activity with $Kp > 6$ was not observed. The low $F_{10.7}$ con-
141 ditions are preferable for the study of SSW effects on the ionosphere. Modeling studies
142 have shown that the ionospheric response to lower atmospheric forcing would be more
143 pronounced under lower solar flux conditions (Fang, Fuller-Rowell, Wang, Akmaev, &
144 Wu, 2014; H.-L. Liu & Richmond, 2013).

145 The EEJ is a narrow band of a zonal electric current that flows along the magnetic
146 equator in the dayside E-region ionosphere at 100–115 km altitude (e.g., Yamazaki & Maute,
147 2017). During geomagnetically quiet periods, day-to-day variations of the EEJ intensity
148 are dominated by the changes in neutral winds at E-region heights associated with at-
149 mospheric waves from the lower layers (Yamazaki et al., 2014), and thus are a good in-
150 dicator of lower-atmospheric influence on the E-region ionosphere. The methods for de-
151 riving the EEJ intensity and equatorial zonal electric field (EEF) from Swarm magnetic
152 field measurements are detailed in Alken, Maus, Vigneron, Sirol, and Hulot (2013). Fig-
153 ure 2a reveals that the EEJ variability was dominated by 6-day variations during this
154 period. The westward phase propagation of the EEJ intensity perturbations with ZW1
155 can also be seen. Similar spatial and temporal variability was found in the equatorial
156 zonal electric field. Figure 2d shows relative changes in the EEF from the time mean.
157 It can be seen that the EEF underwent 6-day variations of $\pm 40\%$ that are out-of-phase
158 for a 180° longitudinal separation. The amplitude varies in the range of 20–70% depend-
159 ing on the longitude. In a recent study, Yamazaki, Stolle, Matzka, and Alken (2018) re-
160 ported that the EEJ intensity occasionally shows ~ 6 -day variations that have charac-
161 teristics of a westward-propagating wave with ZW1. They attributed the EEJ variations
162 to the quasi-6-day wave (Q6DW) that was simultaneously observed in the lower ther-

163 atmosphere. The behavior of the EEJ presented in Figure 2a is similar to those reported
164 by Yamazaki et al. (2018).

165 The Q6DW is a westward-propagating planetary wave with ZW1, which is occa-
166 sionally observed in the middle atmosphere (e.g. Forbes & Zhang, 2017; Hirota & Hi-
167 rooka, 1984; Pancheva, Mukhtarov, & Siskind, 2018; Riggan et al., 2006; Talaat, Yee, &
168 Zhu, 2001, 2002; Wu, Hays, & Skinner, 1994). It is often regarded as the (1,1) Rossby
169 normal mode, which is predicted by classical atmospheric wave theory (Forbes, 1995; Kasa-
170 hara, 1976; Madden, 1979, 2007; Salby, 1984), for its zonal wavenumber, phase speed,
171 and latitudinal structure. The Q6DW can be excited in the troposphere by heating due
172 to moist convection (Miyoshi & Hirooka, 1999). Additionally, the wave can be excited/amplified
173 in the middle atmosphere due to baroclinic/barotropic instability (Lieberman et al., 2003;
174 H.-L. Liu et al., 2004; Meyer & Forbes, 1997). Zonal wind perturbations of the Q6DW
175 are largest around the equator and can be up to a few tens of m/s at E-region heights,
176 which is sufficient to cause detectable changes in dayside ionospheric electric fields and
177 currents (Gan et al., 2016; Miyoshi, 1999; Pedatella, Liu, & Hagan, 2012). These elec-
178 tric field perturbations in the E-region ionosphere are transmitted to the F region along
179 equipotential magnetic field lines, and affect the distribution of low-latitude F-region plas-
180 mas by modulating their $\mathbf{E} \times \mathbf{B}$ plasma drift motions. In this way, the Q6DW can affect
181 the F-region plasma density, as first revealed in the 1990s by ionosonde measurements
182 (e.g., Altadill & Laštovička, 1996; Apostolov, Alberca, & Altadill, 1994; Laštovička, 2006).
183 More recent studies based on global TEC maps have established that the Q6DW effect
184 on the plasma density is largest in the afternoon local time sector near the equatorial
185 ionization anomaly crests ($\pm 20^\circ$ magnetic latitudes) (Gu et al., 2014; Gu, Ruan, et al.,
186 2018; Qin et al., 2019; Yamazaki, 2018).

187 The 6-day variations can be seen in both electron density (Figures 2b and 2e) and
188 top-side TEC (Figures 2c and 2f) at 20° magnetic latitude. (Figure S1 in Supporting
189 Information shows the electron density variations at various latitudes.) The variations
190 are consistent with those in the EEJ/EEF (Figures 2a and 2d), indicating electrodynamic
191 coupling between the E- and F-region ionosphere. The response time of the F-region plasma
192 density to a change in the E-region electric field is 2–4 hours (e.g., Stolle, Manoj, Lühr,
193 Maus, & Alken, 2008; Venkatesh et al., 2015), which would not be visible in the figures.
194 The relative change in the electron density is in the range of 20–40%, which is appre-
195 ciably larger than that of TEC, 5–10%. This is not surprising as the amplitude of the

196 Q6DW decreases with altitude in the top-side ionosphere, as demonstrated by Gu, Ruan,
197 et al. (2018).

198 The plasma density and TEC data from the ascending parts of the Swarm B or-
199 bit (02:00–23:00 MLT) were also examined, but the 6-day variations were not as evident
200 as the results derived from the descending orbits. Similarly, the ionospheric data (EEJ,
201 electron density, and TEC) from Swarm A, which was flying around 02:00–05:00 MLT
202 (descending orbits) and 14:00–17:00 MLT (ascending orbits), did not show strong 6-day
203 variations. The electron density variations from Swarm B (ascending) and Swarm A (as-
204 cending and descending) are presented in Supporting Information (Figure S2). The dif-
205 ferent behavior of 6-day variations in different Swarm datasets reflects the fact that the
206 ionospheric response to the Q6DW depends on MLT and height, as well as on magnetic
207 latitude (Gu, Ruan, et al., 2018). Further studies are required to determine the three
208 dimensional structure of the 6-day ionospheric variations during this event.

209 Previous studies found a significant contribution of the semidiurnal lunar tide to
210 ionospheric variability during NH SSWs (e.g., Park et al., 2012), but it is not known whether
211 the lunar tide plays an equally important role during SH SSWs. The semidiurnal lunar
212 variations in the EEJ intensity derived from the Swarm A and B data during 5 September–
213 5 October 2019 are presented in Supporting Information (Figure S3). It is found that
214 the amplitude of the EEJ semidiurnal lunar variation is 17.7 ± 2.1 mA/m for Swarm A
215 (14:00–17:00 MLT) and 16.6 ± 2.8 mA/m for Swarm B (11:00–14:00 MLT), which is greater
216 than the climatological value of 9.0 ± 0.4 mA/m as reported by Yamazaki et al. (2017)
217 for September daytime (08:00–16:00 local solar time) conditions. The phase, which is de-
218 fined as the lunar time of maximum, is 10.2 ± 0.2 h for Swarm A and 10.0 ± 0.4 h for Swarm
219 B, which is in good agreement with the climatological value of 10.0 ± 0.1 h. Despite the
220 significant enhancement, the lunar variation accounts for only a small part of the observed
221 EEJ variability (compare Figures 2a and S3). The relative amplitude of the semidiur-
222 nal lunar variation in the top-side electron density is $9.9 \pm 0.7\%$ for Swarm A and $11.1 \pm 0.1\%$
223 for Swarm B (also shown in Figure S3). Again, these variations are smaller than the 6-
224 day variations observed during the same period (Figure 2e).

225 It is noted that since Swarm slowly precesses in local solar time, it is not possible
226 to resolve short-term variability of solar tides. Changes in upward-propagating solar tides
227 can occur during SSWs due to changes in the zonal mean atmosphere (Jin et al., 2012;

228 Pedatella & Liu, 2013), tidal sources (Goncharenko, Coster, Plumb, & Domeisen, 2012),
 229 and tidal interaction with PWs (H.-L. Liu, Wang, Richmond, & Roble, 2010; Maute, Ha-
 230 gan, Richmond, & Roble, 2014). Possible changes in solar tides during the September
 231 2019 SSW remain to be investigated.

232 **2.3 Q6DW in the middle atmosphere**

233 Traveling PWs in the middle atmosphere are examined using the GPH data from
 234 Aura/MLS. The analysis method was described in detail in the previous work (Yamazaki
 235 & Matthias, 2019), and thus is only briefly summarized here. The amplitude A and phase
 236 ϕ of waves with period τ were derived by fitting the following formula to the data at a
 237 given latitude and height:

$$238 \sum_{s=-4}^4 A_s \cos \left[2\pi \left(\frac{t}{\tau} + s\lambda \right) - \phi_s \right], \quad (1)$$

239 where t is the universal time, λ is the longitude, and s is the zonal wavenumber. Eastward-
 240 and westward-propagating waves correspond to $s < 0$ and $s > 0$, respectively. The data were
 241 analyzed for each day using a time window that is 3 times the wave period. The $1\text{-}\sigma$ er-
 242 ror in the amplitude is typically below 0.05 km.

243 Figures 3a and 3b show the amplitudes for the westward- and eastward-propagating
 244 waves with ZW1 at 45°S in the lower thermosphere at ~97 km. Enhanced wave activ-
 245 ity can be seen in the westward-propagating component (Figure 3a) with period 4–7d
 246 during September 2019, which can be identified as the Q6DW. It is consistent with the
 247 appearance of 6-day variations in the ionosphere (Figures 2a–2c). Such enhanced wave
 248 activity is not present in the eastward-propagating ZW1 component (Figure 3b), or other
 249 components with higher zonal wavenumbers (not shown here). Although studies have
 250 found that the amplitude of the Q6DW in the middle atmosphere is greatest during equinoc-
 251 tial months (Forbes & Zhang, 2017; Qin et al., 2019; Yamazaki, 2018), the wave enhance-
 252 ment in September 2019 was exceptional, with the maximum amplitude larger than 0.4
 253 km in the lower thermosphere, which is much larger than the climatological amplitude
 254 (0.15 km) or amplitudes recorded during other individual years during 2004–2018 (Fig-
 255 ure 3d). Thus, the large-amplitude Q6DW observed in September 2019 cannot be ex-
 256 plained merely as a seasonal effect.

257 The latitude and height structures of the 6-day wave during 10–30 September 2019
 258 are presented in Figure 3c. The amplitude and phase were derived at wave period of ex-

259 actly 6.0 days, so that the phases calculated at different heights and latitudes can be com-
260 pared. In the mesosphere and lower thermosphere (above 50 km), the amplitude struc-
261 ture is symmetric about the equator with peaks at approximately $\pm 45^\circ$ latitudes, and
262 the phase tends to be horizontally uniform with downward phase progression. These fea-
263 tures are in conformity with the theoretically expected Q6DW in the presence of the mean
264 winds and dissipation (e.g., Salby, 1981a, 1981b). Below 50 km, the phase progression
265 is poleward as well as downward, especially in the SH, indicating equatorward and up-
266 ward energy propagation from the high latitude region. Using reanalysis data, Gan, Ober-
267 heide, and Pedatella (2018) demonstrated how the Q6DW generated in the SH high lat-
268 itude can propagate into the NH, growing to be a global mode in the mesosphere and
269 lower thermosphere under September equinox conditions.

270 In Figure 3c, there is a region of locally enhanced amplitudes at $70\text{--}80^\circ\text{S}$ and 20--
271 50 km altitude, which can be regarded as a source of the large-amplitude Q6DW observed
272 above. The amplification of the Q6DW from the seasonal background in this region is
273 depicted in Figure 3e. Enhanced wave activity is observed in the same region over a wide
274 range of wavenumbers (s from -3 to 3) and periods ($\tau=3\text{--}20\text{d}$) (not shown here). A pos-
275 sible explanation for the wave amplification is baroclinic/barotropic instability (Gan et
276 al., 2018; Lieberman et al., 2003; H.-L. Liu et al., 2004; Meyer & Forbes, 1997), in which
277 waves can rapidly grow by extracting energy from the unstable mean flow. Figure 3f shows
278 that the wave amplification in the polar middle atmosphere is not uncommon around
279 this time of year, but in 2019, it took place at lower altitudes (~ 30 km) than in other
280 years (~ 50 km).

281 Figures 3h–3j illustrates the development of the atmospheric instability. The ar-
282 eas highlighted by the light-yellow color indicate the regions where the necessary con-
283 dition for barotropic/baroclinic instability is met; that is, the meridional gradient of the
284 quasi-geostrophic potential vorticity is negative (e.g., H.-L. Liu et al., 2004). It can be
285 seen that unstable regions are formed mainly around the edge of the polar vortex due
286 to the strong vertical and horizontal shear in the zonal wind. As the westward mean flow
287 descends to lower layers, the unstable regions at high latitudes ($70\text{--}80^\circ\text{S}$) also move down,
288 and hence exciting/amplifying waves at lower altitudes compared to other years. As these
289 waves propagate equatorward and upward, the amplitude at 45°S is greater than other
290 years above ~ 40 km (Figure 3g). As numerically demonstrated by Salby (1981b), the
291 vertical growth of amplitude is enhanced where the zonal mean zonal wind is weak and

292 eastward relative to the phase speed of the wave. The westward phase speed of the Q6DW
293 is ~ 55 m/s at 45°S and ~ 13 m/s at 80°S . Thus, the reduced eastward mean flow and
294 the weak wind reversal during the SSW (Figures 3h–3j) provide favorable conditions for
295 the vertical propagation of the Q6DW. Interactions of the Q6DW with tides and grav-
296 ity waves could also affect the vertical structure of the Q6DW (e.g., Forbes, Zhang, Maute,
297 & Hagan, 2018; Meyer, 1999). A better understanding of the Q6DW propagation in the
298 mesosphere and lower thermosphere during the September 2019 SSW would benefit from
299 a more comprehensive analysis of dynamic fields from an atmospheric reanalysis or gen-
300 eral circulation model.

301 For the NH, possible influence of SSWs on the vertical propagation of traveling plan-
302 etary waves in the middle atmosphere has been discussed in a number of studies (e.g.,
303 Gu, Dou, Pancheva, Yi, & Chen, 2018; Hirooka & Hirota, 1985; Matthias, Hoffmann, Rapp,
304 & Baumgarten, 2012; Pancheva et al., 2008; Sassi, Garcia, & Hoppel, 2012; Yamazaki
305 & Matthias, 2019). In some cases, a strong Q6DW was observed during an SSW (e.g.,
306 Gong et al., 2018; Pancheva et al., 2018) but in general, there is no one-to-one correspon-
307 dence between the occurrence of SSW and Q6DW enhancement in the NH (Yamazaki
308 & Matthias, 2019). Modeling studies also found enhanced Q6DW activity following some
309 SSWs, which has been attributed to barotropic/baroclinic instability in the NH high lat-
310 itude (Chandran, Garcia, Collins, & Chang, 2013; Tomikawa et al., 2012). For the SH,
311 studies are few because of infrequent occurrence of SSWs. Dowdy et al. (2004) and Espy,
312 Hibbins, Riggin, and Fritts (2005) observed a westward-propagating planetary wave with
313 ZW1 and period around 14d at 70–100 km altitude during the September 2002 Antarc-
314 tic SSW. The present study finds a strong response of the Q6DW in the mesosphere and
315 lower thermosphere during the September 2019 Antarctic SSW. It is possible that the
316 response of traveling planetary waves to Antarctic SSWs varies from event to event. More
317 studies are needed to clarify this point.

318 **3 Summary and Conclusions**

319 An SSW occurred in the Southern Hemisphere in September 2019. Although it was
320 a minor warming, it involved an exceptionally strong wave-1 planetary wave and a large
321 polar temperature enhancement by 50.8 K/week. The event also took place under so-
322 lar minimum conditions, which is preferable for studying the ionospheric response. Ear-

323 lier studies focused on the effect of Northern-Hemisphere SSWs on the ionosphere, and
324 few studies investigated Southern-Hemisphere cases.

325 The analysis of ionospheric data from ESA’s Swarm mission during the Septem-
326 ber 2019 SSW reveals prominent 6-day variations in the dayside low-latitude region, in-
327 cluding 20–70% variations in the equatorial zonal electric field, 20–40% variations in the
328 top-side electron density, and 5–10% variations in the top-side total electron content. These
329 variations are attributed to the Q6DW simultaneously observed in the middle atmosphere.
330 Evidence is also found for enhanced lunar tidal perturbations in the ionosphere, but their
331 amplitudes are relatively small (e.g., less than 15% in the top-side electron density).

332 The amplitude of the Q6DW in the lower thermosphere is more than 0.4 km in geopo-
333 tential height, which is found to be the largest observed by Aura/MLS in the Southern
334 Hemisphere since August 2004, and thus cannot be explained merely as a seasonal ef-
335 fect. The latitudinal and vertical structures of the Q6DW suggest that the waves are ex-
336 cited/amplified in the polar region at 30–40 km altitude, where the atmosphere is un-
337 stable due to strong vertical shear in the zonal wind connected with planetary-wave break-
338 ing. As the Q6DW grows in the vertical, the wave attains large amplitudes in the lower
339 thermosphere, which drives ionospheric variability.

340 These results suggest that a Southern-Hemisphere SSW can lead to ionospheric vari-
341 ability by altering middle atmosphere dynamics and propagation characteristics of large-
342 scale waves from the middle atmosphere to the upper atmosphere.

343 **Acknowledgments**

344 We thank the NASA Goddard Earth Sciences (GES) Data and Information Services Cen-
345 ter (DISC) (<https://disc.gsfc.nasa.gov/>) for making the Aura/MLS geopotential height
346 data and MERRA-2 data available. We also thank the European Space Agency (ESA)
347 for providing the Swarm data (<http://earth.esa.int/swarm>). The geomagnetic activity
348 index Kp was provided by the GFZ German Research Centre for Geosciences ([https://www.gfz-
349 potsdam.de/en/kp-index/](https://www.gfz-potsdam.de/en/kp-index/)). The solar activity index $F_{10.7}$ was downloaded from the SPDF
350 OMNIWeb database (<https://omniweb.gsfc.nasa.gov>). This work was supported in part
351 by ESA through contract 4000126709/19/NL/IS “VERA” and by the Deutsche Forschungs-
352 gemeinschaft (DFG) grant YA-574-3-1.

References

- Alken, P., Maus, S., Chulliat, A., Vigneron, P., Sirol, O., & Hulot, G. (2015). Swarm equatorial electric field chain: first results. *Geophysical Research Letters*, *42*(3), 673–680.
- Alken, P., Maus, S., Vigneron, P., Sirol, O., & Hulot, G. (2013). Swarm scarf equatorial electric field inversion chain. *Earth, Planets and Space*, *65*(11), 11.
- Altadill, D., & Laštovička, J., Jan. (1996). Quasi-five-and ten-day oscillations in f0f2 and their possible connection with oscillations at lower ionospheric heights. *Annals of Geophysics*, *39*(4).
- Andrews, D. G., Leovy, C. B., & Holton, J. R. (1987). *Middle atmosphere dynamics* (Vol. 40). Academic press.
- Apostolov, E. M., Alberca, L., & Altadill, D. (1994). Solar cycle and seasonal behaviour of quasi two and rive day oscillations in the time variations of foF2. *Annals of Geophysics*, *37*(2).
- Baldwin, M., Hirooka, T., O’Neill, A., & Yoden, S. (2003). Major stratospheric warming in the southern hemisphere in 2002: Dynamical aspects of the ozone hole split. *SPARC newsletter*, *20*, 24–26.
- Buchert, S., Zangerl, F., Sust, M., André, M., Eriksson, A., Wahlund, J.-E., & Opgenoorth, H. (2015). Swarm observations of equatorial electron densities and topside gps track losses. *Geophysical Research Letters*, *42*(7), 2088–2092.
- Butler, A. H., Seidel, D. J., Hardiman, S. C., Butchart, N., Birner, T., & Match, A. (2015). Defining sudden stratospheric warmings. *Bulletin of the American Meteorological Society*, *96*(11), 1913–1928.
- Cámara, A. d. l., Albers, J. R., Birner, T., Garcia, R. R., Hitchcock, P., Kinnison, D. E., & Smith, A. K. (2017). Sensitivity of sudden stratospheric warmings to previous stratospheric conditions. *Journal of the Atmospheric Sciences*, *74*(9), 2857–2877.
- Chandran, A., Collins, R., & Harvey, V. (2014). Stratosphere-mesosphere coupling during stratospheric sudden warming events. *Advances in Space Research*, *53*(9), 1265–1289.
- Chandran, A., Garcia, R., Collins, R., & Chang, L. (2013). Secondary planetary waves in the middle and upper atmosphere following the stratospheric sudden warming event of January 2012. *Geophysical Research Letters*, *40*(9),

- 386 1861–1867.
- 387 Charlton, A. J., & Polvani, L. M. (2007). A new look at stratospheric sudden
388 warmings. Part I: Climatology and modeling benchmarks. *Journal of Climate*,
389 *20*(3), 449–469.
- 390 Chau, J., Aponte, N., Cabassa, E., Sulzer, M., Goncharenko, L. P., & González, S.
391 (2010). Quiet time ionospheric variability over arecibo during sudden strato-
392 spheric warming events. *Journal of Geophysical Research: Space Physics*,
393 *115*(A9).
- 394 Chau, J., Goncharenko, L. P., Fejer, B. G., & Liu, H.-L. (2012). Equatorial and low
395 latitude ionospheric effects during sudden stratospheric warming events. *Space*
396 *Science Reviews*, *168*(1-4), 385–417.
- 397 Chau, J., Hoffmann, P., Pedatella, N., Matthias, V., & Stober, G. (2015). Upper
398 mesospheric lunar tides over middle and high latitudes during sudden strato-
399 spheric warming events. *Journal of Geophysical Research: Space Physics*,
400 *120*(4), 3084–3096.
- 401 Dowdy, A. J., Vincent, R. A., Murphy, D. J., Tsutsumi, M., Riggin, D. M., & Jarvis,
402 M. J. (2004). The large-scale dynamics of the mesosphere–lower thermosphere
403 during the southern hemisphere stratospheric warming of 2002. *Geophysical*
404 *Research Letters*, *31*(14).
- 405 Espy, P., Hibbins, R., Riggin, D., & Fritts, D. (2005). Mesospheric planetary waves
406 over antarctica during 2002. *Geophysical Research Letters*, *32*(21).
- 407 Fang, T.-W., Fuller-Rowell, T., Akmaev, R., Wu, F., Wang, H., & Anderson, D.
408 (2012). Longitudinal variation of ionospheric vertical drifts during the 2009
409 sudden stratospheric warming. *Journal of Geophysical Research: Space*
410 *Physics*, *117*(A3).
- 411 Fang, T.-W., Fuller-Rowell, T., Wang, H., Akmaev, R., & Wu, F. (2014). Iono-
412 spheric response to sudden stratospheric warming events at low and high solar
413 activity. *Journal of Geophysical Research: Space Physics*, *119*(9), 7858–7869.
- 414 Fejer, B. G., Olson, M., Chau, J., Stolle, C., Lühr, H., Goncharenko, L. P., . . . Na-
415 gatsuma, T. (2010). Lunar-dependent equatorial ionospheric electrodynamic
416 effects during sudden stratospheric warmings. *Journal of Geophysical Research:*
417 *Space Physics*, *115*(A8).
- 418 Fejer, B. G., Tracy, B., Olson, M., & Chau, J. (2011). Enhanced lunar semidiurnal

- 419 equatorial vertical plasma drifts during sudden stratospheric warmings. *Geo-*
420 *physical Research Letters*, *38*(21).
- 421 Forbes, J. M. (1995). Tidal and planetary waves. *The upper mesosphere and lower*
422 *thermosphere: a review of experiment and theory*, *87*, 67–87.
- 423 Forbes, J. M., & Zhang, X. (2012). Lunar tide amplification during the January
424 2009 stratosphere warming event: Observations and theory. *Journal of Geo-*
425 *physical Research: Space Physics*, *117*(A12).
- 426 Forbes, J. M., & Zhang, X. (2017). The quasi-6 day wave and its interactions with
427 solar tides. *Journal of Geophysical Research: Space Physics*, *122*(4), 4764–
428 4776.
- 429 Forbes, J. M., Zhang, X., Maute, A., & Hagan, M. E. (2018). Zonally symmetric os-
430 cillations of the thermosphere at planetary wave periods. *Journal of Geophysi-*
431 *cal Research: Space Physics*, *123*(5), 4110–4128.
- 432 Friis-Christensen, E., Lühr, H., & Hulot, G. (2006). Swarm: A constellation to study
433 the earth’s magnetic field. *Earth, planets and space*, *58*(4), 351–358.
- 434 Friis-Christensen, E., Lühr, H., Knudsen, D., & Haagmans, R. (2008). Swarm—an
435 earth observation mission investigating geospace. *Advances in Space Research*,
436 *41*(1), 210–216.
- 437 Fuller-Rowell, T., Wang, H., Akmaev, R., Wu, F., Fang, T.-W., Iredell, M., & Rich-
438 mond, A. (2011). Forecasting the dynamic and electrodynamic response to
439 the January 2009 sudden stratospheric warming. *Geophysical Research Letters*,
440 *38*(13).
- 441 Gan, Q., Oberheide, J., & Pedatella, N. M. (2018). Sources, sinks, and propagation
442 characteristics of the quasi 6-day wave and its impact on the residual mean cir-
443 culation. *Journal of Geophysical Research: Atmospheres*, *123*(17), 9152–9170.
- 444 Gan, Q., Wang, W., Yue, J., Liu, H., Chang, L. C., Zhang, S., . . . Du, J. (2016).
445 Numerical simulation of the 6 day wave effects on the ionosphere: Dynamo
446 modulation. *Journal of Geophysical Research: Space Physics*, *121*(10), 10–
447 103.
- 448 Gelaro, R., McCarty, W., Suárez, M. J., Todling, R., Molod, A., Takacs, L., . . .
449 others (2017). The modern-era retrospective analysis for research and applica-
450 tions, version 2 (MERRA-2). *Journal of Climate*, *30*(14), 5419–5454.
- 451 Goncharenko, L. P., Chau, J., Liu, H.-L., & Coster, A. (2010). Unexpected connec-

- 452 tions between the stratosphere and ionosphere. *Geophysical Research Letters*,
453 37(10).
- 454 Goncharenko, L. P., Coster, A., Chau, J., & Valladares, C. (2010). Impact of sudden
455 stratospheric warmings on equatorial ionization anomaly. *Journal of Geophysical
456 Research: Space Physics*, 115(A10).
- 457 Goncharenko, L. P., Coster, A., Plumb, R. A., & Domeisen, D. I. (2012). The poten-
458 tial role of stratospheric ozone in the stratosphere-ionosphere coupling during
459 stratospheric warmings. *Geophysical Research Letters*, 39(8).
- 460 Gong, Y., Li, C., Ma, Z., Zhang, S., Zhou, Q., Huang, C., . . . Ning, B. (2018). Study
461 of the quasi-5-day wave in the mlt region by a meteor radar chain. *Journal of
462 Geophysical Research: Atmospheres*, 123(17), 9474–9487.
- 463 Gu, S.-Y., Dou, X., Pancheva, D., Yi, W., & Chen, T. (2018). Investigation of the
464 abnormal quasi 2-day wave activities during the sudden stratospheric warm-
465 ing period of January 2006. *Journal of Geophysical Research: Space Physics*,
466 123(7), 6031–6041.
- 467 Gu, S.-Y., Liu, H.-L., Li, T., Dou, X., Wu, Q., & Russell III, J. M. (2014). Observa-
468 tion of the neutral-ion coupling through 6 day planetary wave. *Journal of Geo-
469 physical Research: Space Physics*, 119(12), 10–376.
- 470 Gu, S.-Y., Ruan, H., Yang, C.-Y., Gan, Q., Dou, X., & Wang, N. (2018). The
471 morphology of the 6-day wave in both the neutral atmosphere and f region
472 ionosphere under solar minimum conditions. *Journal of Geophysical Research:
473 Space Physics*, 123(5), 4232–4240.
- 474 Hirooka, T., & Hirota, I. (1985). Normal mode rossby waves observed in the upper
475 stratosphere. Part II: Second antisymmetric and symmetric modes of zonal
476 wavenumbers 1 and 2. *Journal of the atmospheric sciences*, 42(6), 536–548.
- 477 Hirota, I., & Hirooka, T. (1984). Normal mode rossby waves observed in the upper
478 stratosphere. Part I: First symmetric modes of zonal wavenumbers 1 and 2.
479 *Journal of the atmospheric sciences*, 41(8), 1253–1267.
- 480 Jin, H., Miyoshi, Y., Pancheva, D., Mukhtarov, P., Fujiwara, H., & Shinagawa, H.
481 (2012). Response of migrating tides to the stratospheric sudden warming
482 in 2009 and their effects on the ionosphere studied by a whole atmosphere-
483 ionosphere model GAIA with COSMIC and TIMED/SABER observations.
484 *Journal of Geophysical Research: Space Physics*, 117(A10).

- 485 Kasahara, A. (1976). Normal modes of ultralong waves in the atmosphere. *Monthly*
486 *Weather Review*, *104*(6), 669–690.
- 487 Krüger, K., Naujokat, B., & Labitzke, K. (2005). The unusual midwinter warm-
488 ing in the southern hemisphere stratosphere 2002: A comparison to northern
489 hemisphere phenomena. *Journal of the atmospheric sciences*, *62*(3), 603–613.
- 490 Labitzke, K., & Van Loon, H. (1999). *The stratosphere: phenomena, history, and*
491 *relevance*. Springer Science & Business Media.
- 492 Laštovička, J. (2006). Forcing of the ionosphere by waves from below. *Journal of At-*
493 *mospheric and Solar-Terrestrial Physics*, *68*(3-5), 479–497.
- 494 Lieberman, R., Riggan, D., Franke, S., Manson, A., Meek, C., Nakamura, T., . . .
495 Reid, I. (2003). The 6.5-day wave in the mesosphere and lower thermosphere:
496 Evidence for baroclinic/barotropic instability. *Journal of Geophysical Research:*
497 *Atmospheres*, *108*(D20).
- 498 Limpasuvan, V., Thompson, D. W., & Hartmann, D. L. (2004). The life cycle of
499 the northern hemisphere sudden stratospheric warmings. *Journal of Climate*,
500 *17*(13), 2584–2596.
- 501 Lin, J.-T., Lin, C., Lin, C., Pedatella, N. M., Rajesh, P., Matsuo, T., & Liu, J.
502 (2019). Revisiting the modulations of ionospheric solar and lunar migrating
503 tides during the 2009 stratospheric sudden warming by using global ionosphere
504 specification. *Space Weather*, *17*(5), 767–777.
- 505 Liu, H., Yamamoto, M., Tulası Ram, S., Tsugawa, T., Otsuka, Y., Stolle, C., . . .
506 Nagatsuma, T. (2011). Equatorial electrodynamics and neutral background
507 in the asian sector during the 2009 stratospheric sudden warming. *Journal of*
508 *Geophysical Research: Space Physics*, *116*(A8).
- 509 Liu, H.-L., & Richmond, A. (2013). Attribution of ionospheric vertical plasma drift
510 perturbations to large-scale waves and the dependence on solar activity. *Jour-*
511 *nal of Geophysical Research: Space Physics*, *118*(5), 2452–2465.
- 512 Liu, H.-L., Talaat, E., Roble, R., Lieberman, R., Riggan, D., & Yee, J.-H. (2004).
513 The 6.5-day wave and its seasonal variability in the middle and upper atmo-
514 sphere. *Journal of Geophysical Research: Atmospheres*, *109*(D21).
- 515 Liu, H.-L., Wang, W., Richmond, A., & Roble, R. (2010). Ionospheric variabil-
516 ity due to planetary waves and tides for solar minimum conditions. *Journal of*
517 *Geophysical Research: Space Physics*, *115*(A6).

- 518 Liu, J., Zhang, D.-H., Hao, Y.-Q., & Xiao, Z. (2019). The comparison of lunar tidal
 519 characteristics in the low-latitudinal ionosphere between east asian and ameri-
 520 can sectors during stratospheric sudden warming events: 2009-2018. *Journal of*
 521 *Geophysical Research: Space Physics*.
- 522 Madden, R. A. (1979). Observations of large-scale traveling rossby waves. *Reviews of*
 523 *Geophysics*, 17(8), 1935–1949.
- 524 Madden, R. A. (2007). Large-scale, free rossby waves in the atmosphere—an update.
 525 *Tellus A: Dynamic Meteorology and Oceanography*, 59(5), 571–590.
- 526 Matsuno, T. (1971). A dynamical model of the stratospheric sudden warming. *Jour-*
 527 *nal of the Atmospheric Sciences*, 28(8), 1479–1494.
- 528 Matthias, V., & Ern, M. (2018). On the origin of the mesospheric quasi-stationary
 529 planetary waves in the unusual arctic winter 2015/2016. *Atmospheric Chem-*
 530 *istry and Physics*, 18(7), 4803–4815.
- 531 Matthias, V., Hoffmann, P., Rapp, M., & Baumgarten, G. (2012). Composite
 532 analysis of the temporal development of waves in the polar mlt region during
 533 stratospheric warmings. *Journal of Atmospheric and Solar-Terrestrial Physics*,
 534 90, 86–96.
- 535 Maute, A., Hagan, M., Richmond, A., & Roble, R. (2014). TIME-GCM study of
 536 the ionospheric equatorial vertical drift changes during the 2006 stratospheric
 537 sudden warming. *Journal of Geophysical Research: Space Physics*, 119(2),
 538 1287–1305.
- 539 McInturff, R. M. (1978). *Stratospheric warmings: Synop-*
 540 *tic, dynamic and general-circulation aspects* (Tech. Rep. No.
 541 Ref. Publ. 1017). Suitland, Md.. (available online at
 542 <https://ntrs.nasa.gov/archive/nasa/casi.ntrs.nasa.gov/19780010687.pdf>)
- 543 McIntyre, M. E. (1982). How well do we understand the dynamics of stratospheric
 544 warmings? *Journal of the Meteorological Society of Japan. Ser. II*, 60(1), 37–
 545 65.
- 546 Meyer, C. K. (1999). Gravity wave interactions with mesospheric planetary waves:
 547 A mechanism for penetration into the thermosphere-ionosphere system. *Jour-*
 548 *nal of Geophysical Research: Space Physics*, 104(A12), 28181–28196.
- 549 Meyer, C. K., & Forbes, J. M. (1997). A 6.5-day westward propagating planetary
 550 wave: Origin and characteristics. *Journal of Geophysical Research: Atmo-*

- 551 *spheres*, 102(D22), 26173–26178.
- 552 Miyoshi, Y. (1999). Numerical simulation of the 5-day and 16-day waves in the
553 mesopause region. *Earth, planets and space*, 51(7-8), 763–772.
- 554 Miyoshi, Y., & Hirooka, T. (1999). A numerical experiment of excitation of the 5-
555 day wave by a GCM. *Journal of the atmospheric sciences*, 56(11), 1698–1707.
- 556 Nayak, C., & Yiğit, E. (2019). Variation of small-scale gravity wave activity in
557 the ionosphere during the major sudden stratospheric warming event of 2009.
558 *Journal of Geophysical Research: Space Physics*, 124(1), 470–488.
- 559 Olson, M., Fejer, B., Stolle, C., Lühr, H., & Chau, J. (2013). Equatorial iono-
560 spheric electrodynamic perturbations during southern hemisphere stratospheric
561 warming events. *Journal of Geophysical Research: Space Physics*, 118(3),
562 1190–1195.
- 563 Oyama, K.-I., Jhou, J., Lin, J., Lin, C., Liu, H., & Yumoto, K. (2014). Ionospheric
564 response to 2009 sudden stratospheric warming in the northern hemisphere.
565 *Journal of Geophysical Research: Space Physics*, 119(12), 10–260.
- 566 Pancheva, D., & Mukhtarov, P. (2011). Stratospheric warmings: The atmosphere–
567 ionosphere coupling paradigm. *Journal of Atmospheric and Solar-Terrestrial*
568 *Physics*, 73(13), 1697–1702.
- 569 Pancheva, D., Mukhtarov, P., Mitchell, N., Merzlyakov, E., Smith, A., Andonov,
570 B., . . . others (2008). Planetary waves in coupling the stratosphere and
571 mesosphere during the major stratospheric warming in 2003/2004. *Journal of*
572 *Geophysical Research: Atmospheres*, 113(D12).
- 573 Pancheva, D., Mukhtarov, P., & Siskind, D. E. (2018). The quasi-6-day waves in
574 nogaps-alpha forecast model and their climatology in mls/aura measurements
575 (2005–2014). *Journal of Atmospheric and Solar-Terrestrial Physics*, 181,
576 19–37.
- 577 Park, J., Lühr, H., Kervalishvili, G., Rauberg, J., Stolle, C., Kwak, Y.-S., & Lee,
578 W. K. (2017). Morphology of high-latitude plasma density perturbations as
579 deduced from the total electron content measurements onboard the swarm
580 constellation. *Journal of Geophysical Research: Space Physics*, 122(1), 1338–
581 1359.
- 582 Park, J., Lühr, H., Kunze, M., Fejer, B. G., & Min, K. W. (2012). Effect of sudden
583 stratospheric warming on lunar tidal modulation of the equatorial electrojet.

- 584 *Journal of Geophysical Research: Space Physics*, 117(A3).
- 585 Patra, A., Pavan Chaitanya, P., Sripathi, S., & Alex, S. (2014). Ionospheric vari-
586 ability over Indian low latitude linked with the 2009 sudden stratospheric
587 warming. *Journal of Geophysical Research: Space Physics*, 119(5), 4044–4061.
- 588 Pedatella, N., Chau, J., Schmidt, H., Goncharenko, L., Stolle, C., Hocke, K., . . .
589 Siddiqui, T. (2018). How sudden stratospheric warming affects the whole
590 atmosphere. *Eos*, 99, 35–38.
- 591 Pedatella, N., & Forbes, J. (2010). Evidence for stratosphere sudden warming-
592 ionosphere coupling due to vertically propagating tides. *Geophysical Research*
593 *Letters*, 37(11).
- 594 Pedatella, N., & Liu, H.-L. (2013). The influence of atmospheric tide and planetary
595 wave variability during sudden stratosphere warmings on the low latitude iono-
596 sphere. *Journal of Geophysical Research: Space Physics*, 118(8), 5333–5347.
- 597 Pedatella, N., Liu, H.-L., & Hagan, M. (2012). Day-to-day migrating and nonmigrat-
598 ing tidal variability due to the six-day planetary wave. *Journal of Geophysical*
599 *Research: Space Physics*, 117(A6).
- 600 Pedatella, N., Liu, H.-L., Sassi, F., Lei, J., Chau, J., & Zhang, X. (2014). Ionosphere
601 variability during the 2009 SSW: Influence of the lunar semidiurnal tide and
602 mechanisms producing electron density variability. *Journal of Geophysical*
603 *Research: Space Physics*, 119(5), 3828–3843.
- 604 Pedatella, N., & Maute, A. (2015). Impact of the semidiurnal lunar tide on the
605 midlatitude thermospheric wind and ionosphere during sudden stratosphere
606 warmings. *Journal of Geophysical Research: Space Physics*, 120(12), 10–740.
- 607 Qin, Y., Gu, S.-Y., Dou, X., Gong, Y., Chen, G., Zhang, S., & Wu, Q. (2019). Cli-
608 matology of the quasi-6-day wave in the mesopause region and its modulations
609 on total electron content during 2003–2017. *Journal of Geophysical Research:*
610 *Space Physics*, 124(1), 573–583.
- 611 Riggan, D. M., Liu, H.-L., Lieberman, R. S., Roble, R. G., Russell III, J. M.,
612 Mertens, C. J., . . . others (2006). Observations of the 5-day wave in the meso-
613 sphere and lower thermosphere. *Journal of Atmospheric and Solar-Terrestrial*
614 *Physics*, 68(3-5), 323–339.
- 615 Rodrigues, F., Crowley, G., Azeem, S., & Heelis, R. (2011). C/nofs observations
616 of the equatorial ionospheric electric field response to the 2009 major sudden

- 617 stratospheric warming event. *Journal of Geophysical Research: Space Physics*,
618 *116*(A9).
- 619 Salby, M. L. (1981a). Rossby normal modes in nonuniform background configura-
620 tions. Part II. equinox and solstice conditions. *Journal of the Atmospheric Sci-*
621 *ences*, *38*(9), 1827–1840.
- 622 Salby, M. L. (1981b). Rossby normal modes in nonuniform background configura-
623 tions. Part I: Simple fields. *Journal of the Atmospheric Sciences*, *38*(9), 1803–
624 1826.
- 625 Salby, M. L. (1984). Survey of planetary-scale traveling waves: The state of theory
626 and observations. *Reviews of Geophysics*, *22*(2), 209–236.
- 627 Sassi, F., Garcia, R., & Hoppel, K. (2012). Large-scale rossby normal modes dur-
628 ing some recent northern hemisphere winters. *Journal of the Atmospheric Sci-*
629 *ences*, *69*(3), 820–839.
- 630 Sassi, F., Liu, H.-L., Ma, J., & Garcia, R. R. (2013). The lower thermosphere during
631 the northern hemisphere winter of 2009: A modeling study using high-altitude
632 data assimilation products in WACCM-X. *Journal of Geophysical Research:*
633 *Atmospheres*, *118*(16), 8954–8968.
- 634 Schwartz, M., Lambert, A., Manney, G., Read, W., Livesey, N., Froidevaux, L., . . .
635 others (2008). Validation of the aura microwave limb sounder temperature
636 and geopotential height measurements. *Journal of Geophysical Research:*
637 *Atmospheres*, *113*(D15).
- 638 Siddiqui, T. A., Maute, A., Pedatella, N., Yamazaki, Y., Lühr, H., & Stolle, C.
639 (2018). On the variability of the semidiurnal solar and lunar tides of the equa-
640 torial electrojet during sudden stratospheric warmings. In *Annales geophysicae*
641 (Vol. 36, pp. 1545–1562).
- 642 Siddiqui, T. A., Stolle, C., Lühr, H., & Matzka, J. (2015). On the relationship be-
643 tween weakening of the northern polar vortex and the lunar tidal amplification
644 in the equatorial electrojet. *Journal of Geophysical Research: Space Physics*,
645 *120*(11), 10006–10019.
- 646 Stening, R., Forbes, J., Hagan, M., & Richmond, A. (1997). Experiments with a
647 lunar atmospheric tidal model. *Journal of Geophysical Research: Atmospheres*,
648 *102*(D12), 13465–13471.
- 649 Stolle, C., Manoj, C., Lühr, H., Maus, S., & Alken, P. (2008). Estimating the day-

- 650 time equatorial ionization anomaly strength from electric field proxies. *Journal*
651 *of Geophysical Research: Space Physics*, 113(A9).
- 652 Talaat, E., Yee, J.-H., & Zhu, X. (2001). Observations of the 6.5-day wave in the
653 mesosphere and lower thermosphere. *Journal of Geophysical Research: Atmo-*
654 *spheres*, 106(D18), 20715–20723.
- 655 Talaat, E., Yee, J.-H., & Zhu, X. (2002). The 6.5-day wave in the tropical strato-
656 sphere and mesosphere. *Journal of Geophysical Research: Atmospheres*,
657 107(D12), ACL–1.
- 658 Tomikawa, Y., Sato, K., Watanabe, S., Kawatani, Y., Miyazaki, K., & Takahashi,
659 M. (2012). Growth of planetary waves and the formation of an elevated
660 stratopause after a major stratospheric sudden warming in a T213L256 GCM.
661 *Journal of Geophysical Research: Atmospheres*, 117(D16).
- 662 Venkatesh, K., Fagundes, P., Prasad, D. V., Denardini, C. M., De Abreu, A., De Je-
663 sus, R., & Gende, M. (2015). Day-to-day variability of equatorial electro-
664 jet and its role on the day-to-day characteristics of the equatorial ionization
665 anomaly over the indian and brazilian sectors. *Journal of Geophysical Re-*
666 *search: Space Physics*, 120(10), 9117–9131.
- 667 Wang, H., Akmaev, R., Fang, T.-W., Fuller-Rowell, T., Wu, F., Maruyama, N., &
668 Iredell, M. (2014). First forecast of a sudden stratospheric warming with a
669 coupled whole-atmosphere/ionosphere model idea. *Journal of Geophysical*
670 *Research: Space Physics*, 119(3), 2079–2089.
- 671 Waters, J. W., Froidevaux, L., Harwood, R. S., Jarnot, R. F., Pickett, H. M., Read,
672 W. G., . . . others (2006). The earth observing system microwave limb sounder
673 (eos mls) on the aura satellite. *IEEE Transactions on Geoscience and Remote*
674 *Sensing*, 44(5), 1075–1092.
- 675 Wu, D., Hays, P., & Skinner, W. (1994). Observations of the 5-day wave in the
676 mesosphere and lower thermosphere. *Geophysical Research Letters*, 21(24),
677 2733–2736.
- 678 Yadav, S., Pant, T. K., Choudhary, R., Vineeth, C., Sunda, S., Kumar, K., . . .
679 Mukherjee, S. (2017). Impact of sudden stratospheric warming of 2009 on the
680 equatorial and low-latitude ionosphere of the indian longitudes: A case study.
681 *Journal of Geophysical Research: Space Physics*, 122(10), 10–486.
- 682 Yamazaki, Y. (2018). Quasi-6-day wave effects on the equatorial ionization anomaly

- 683 over a solar cycle. *Journal of Geophysical Research: Space Physics*, *123*(11),
684 9881–9892.
- 685 Yamazaki, Y., & Matthias, V. (2019). Large-amplitude quasi-10-day waves in
686 the middle atmosphere during final warmings. *Journal of Geophysical Re-*
687 *search: Atmospheres*, *124*(17-18), 9874-9892. Retrieved from [https://](https://agupubs.onlinelibrary.wiley.com/doi/abs/10.1029/2019JD030634)
688 agupubs.onlinelibrary.wiley.com/doi/abs/10.1029/2019JD030634 doi:
689 10.1029/2019JD030634
- 690 Yamazaki, Y., & Maute, A. (2017). Sq and eej—a review on the daily variation
691 of the geomagnetic field caused by ionospheric dynamo currents. *Space Science*
692 *Reviews*, *206*(1-4), 299–405.
- 693 Yamazaki, Y., Richmond, A., Maute, A., Liu, H.-L., Pedatella, N., & Sassi, F.
694 (2014). On the day-to-day variation of the equatorial electrojet during quiet
695 periods. *Journal of Geophysical Research: Space Physics*, *119*(8), 6966–6980.
- 696 Yamazaki, Y., Richmond, A., & Yumoto, K. (2012). Stratospheric warmings and the
697 geomagnetic lunar tide: 1958–2007. *Journal of Geophysical Research: Space*
698 *Physics*, *117*(A4).
- 699 Yamazaki, Y., Stolle, C., Matzka, J., & Alken, P. (2018). Quasi-6-day wave mod-
700 ulation of the equatorial electrojet. *Journal of Geophysical Research: Space*
701 *Physics*, *123*(5), 4094–4109.
- 702 Yamazaki, Y., Stolle, C., Matzka, J., Siddiqui, T. A., Lühr, H., & Alken, P. (2017).
703 Longitudinal variation of the lunar tide in the equatorial electrojet. *Journal of*
704 *Geophysical Research: Space Physics*, *122*(12), 12–445.
- 705 Yue, X., Schreiner, W. S., Lei, J., Rocken, C., Hunt, D. C., Kuo, Y.-H., & Wan, W.
706 (2010). Global ionospheric response observed by COSMIC satellites during
707 the January 2009 stratospheric sudden warming event. *Journal of Geophysical*
708 *Research: Space Physics*, *115*(A11).
- 709 Zhang, X., & Forbes, J. M. (2014). Lunar tide in the thermosphere and weakening of
710 the northern polar vortex. *Geophysical Research Letters*, *41*(23), 8201–8207.

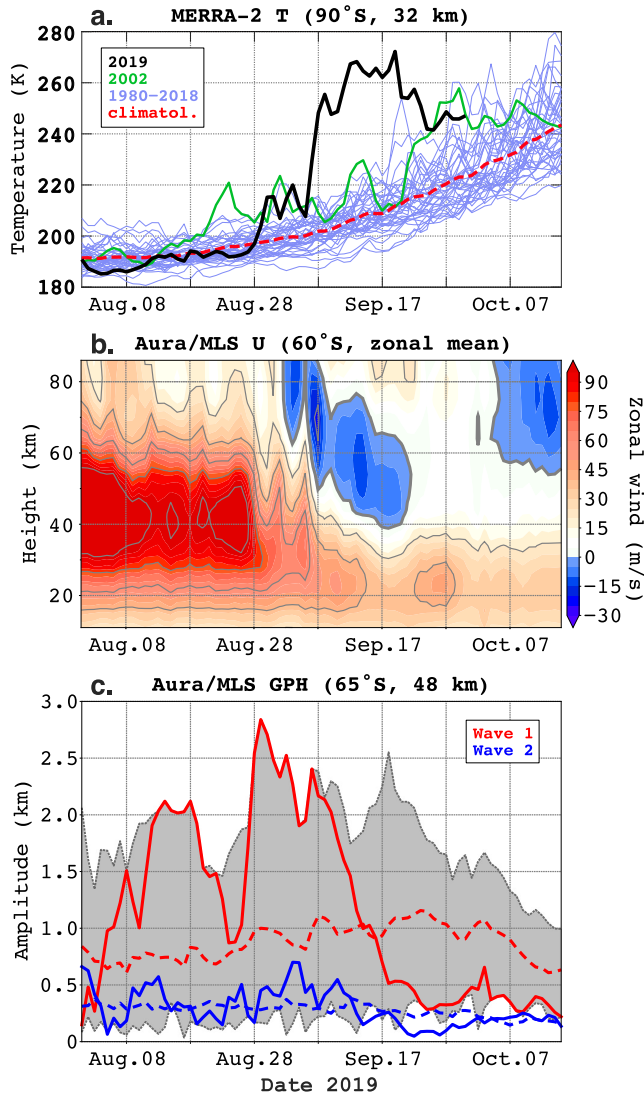


Figure 1. Overview of middle atmosphere dynamics during the September 2019 sudden stratospheric warming. (a) Stratospheric polar temperature at 10 hPa obtained from the MERRA-2 reanalysis. The thick black line represents the data for 2019, while the thin purple lines correspond to the data for other years during 1980–2018, among which the data for 2002 are highlighted by green for the occurrence of a major SSW. The red dashed line shows the climatological mean. (b) Zonal mean zonal wind at 60°S derived from the geopotential height (GPH) measurements by the Aura Microwave Limb Sounder (MLS) using the method described by Matthias and Ern (2018). (c) Amplitude of the planetary wave with Zonal Wavenumber (ZW) 1 and ZW2 at 65°S and 48 km altitude from the Aura/MLS GPH. The red and blue solid lines represent ZW1 and ZW2 waves, respectively. The climatological amplitudes of the ZW1 and ZW2 waves are indicated by the dashed lines with corresponding colors. The gray shaded area show the range between the maximum and minimum values of the amplitude of the ZW1 wave observed by Aura/MLS since August 2004. –24–

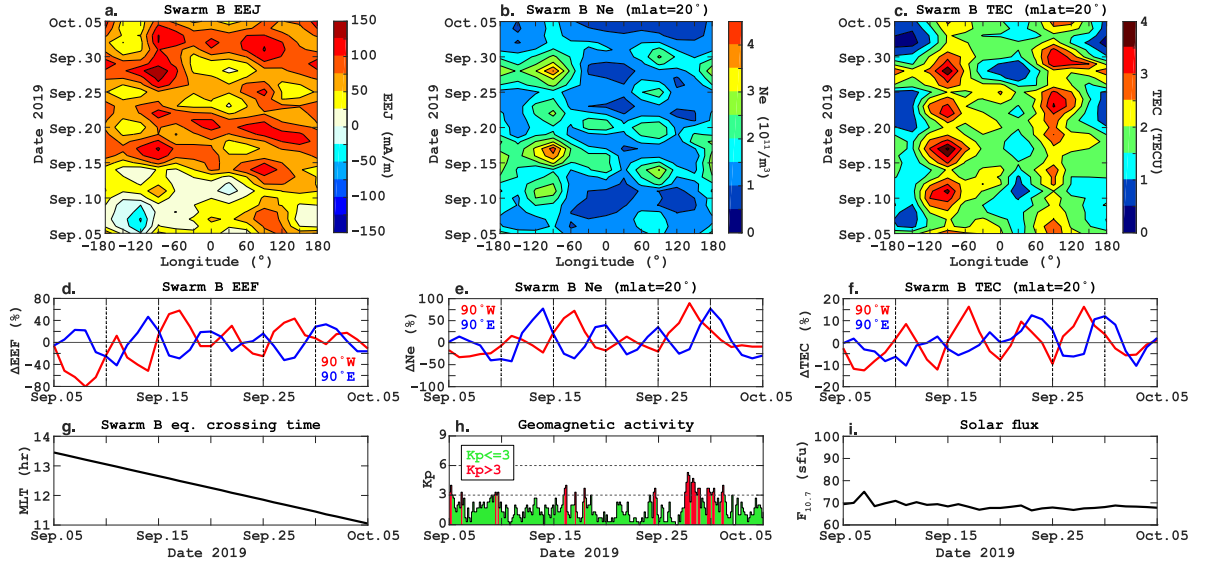


Figure 2. Overview of ionospheric variations during 5 September–5 October 2019. (a) Longitude versus time plot of the equatorial electrojet (EEJ) intensity derived from magnetic field measurements in the descending orbits of Swarm B. The data are smoothed using a 3-day and 50°-longitude window. (b) Same as (a) except for the electron density at 20° magnetic latitude. (c) Same as (a) except for the total electron content (TEC) at 20° magnetic latitude at the satellite altitude of ~510 km. (d) Percent changes in the Swarm B zonal equatorial electric field (EEF) at $\pm 90^\circ$ longitudes with respect to the time mean at the corresponding longitudes. (e) Same as (d) except for the Swarm B electron density at 20° magnetic latitude. (f) Same as (d) except for the Swarm B TEC at 20° magnetic latitude. (g) Magnetic local time (MLT) at equatorial crossings for the descending orbits of Swarm B. (h) Geomagnetic activity index Kp . (i) Solar activity index $F_{10.7}$.

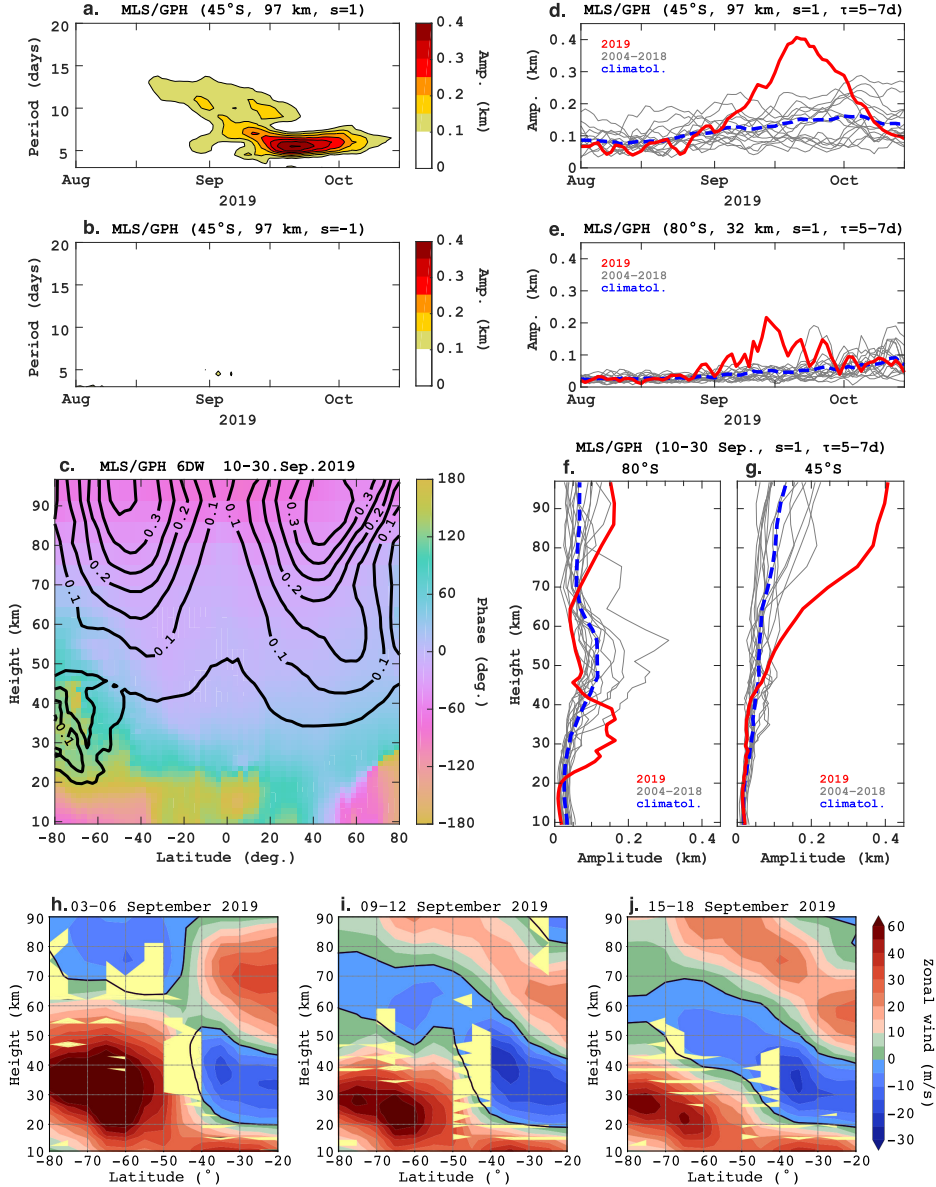


Figure 3. Overview of quasi-6-day wave (Q6DW) activity during the September 2019 SSW as derived from the geopotential height (GPH) measurements by the Aura Microwave Limb Sounder (MLS). (a) Amplitude of the westward-propagating Zonal Wavenumber (ZW) 1 waves at 45°S and 97 km altitude. (b) Same as (a) except for the eastward-propagating ZW1 waves. (c) Latitude versus height structures of the westward-propagating ZW1 wave with period 6.0d during 10–30 September 2019. The contour lines indicate the amplitude while the color represents the phase. (d) Amplitude of the Q6DW, defined here as the maximum amplitude of the westward-propagating ZW1 waves at periods 5–7d, at 45°S and 97 km altitude. (e) Same as (d) except at 80°S and 32 km altitude. (f) Vertical structure of the Q6DW at 80°S during 10–30 September 2019. (g) Same as (f) except at 45°S. (h–j) Latitude versus height structures of the zonal mean zonal wind. The areas highlighted by the light-yellow color indicate the regions where the meridional gradient of the quasi-geostrophic potential vorticity is negative, which is the necessary condition for barotropic/baroclinic instability.

Figure 1.

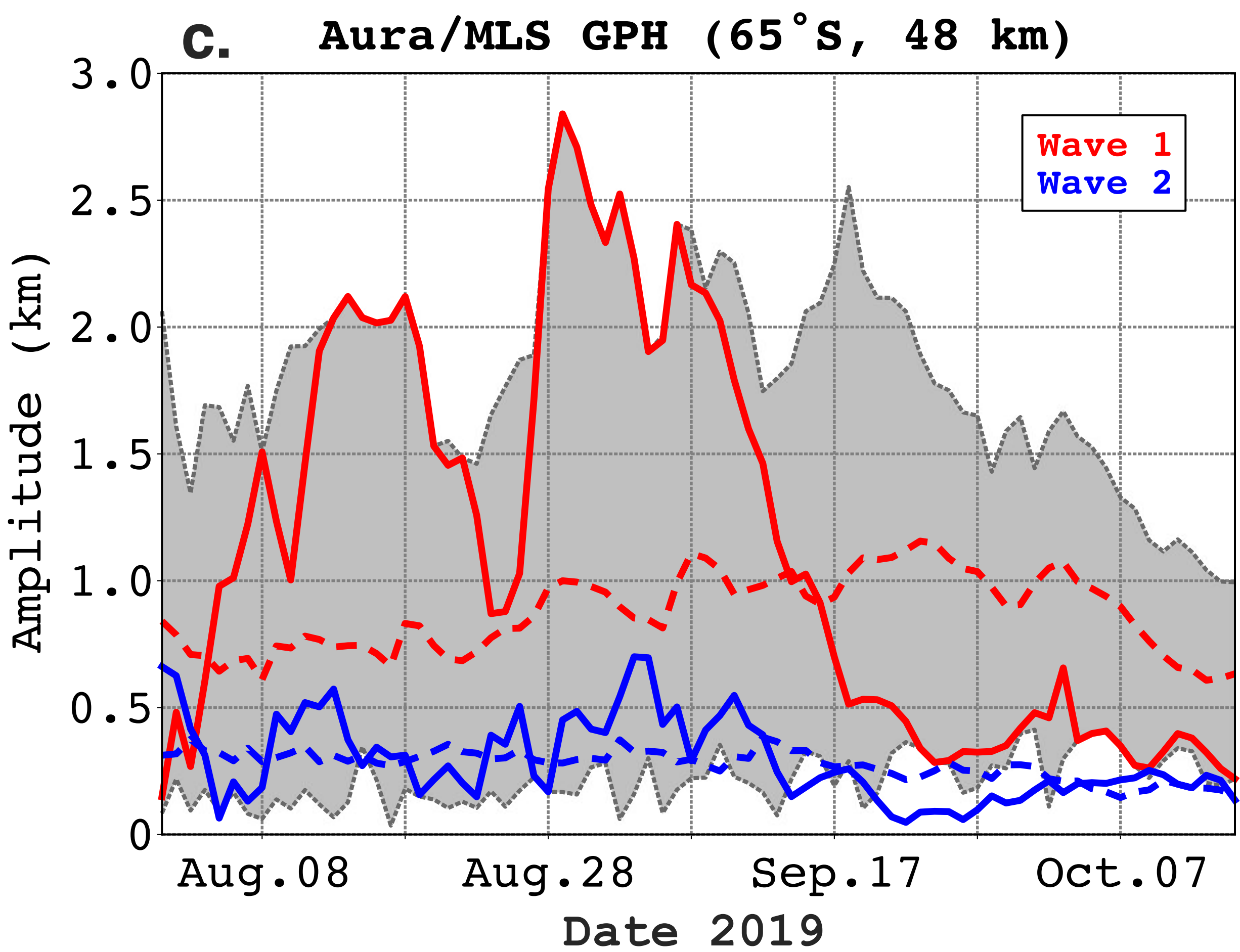
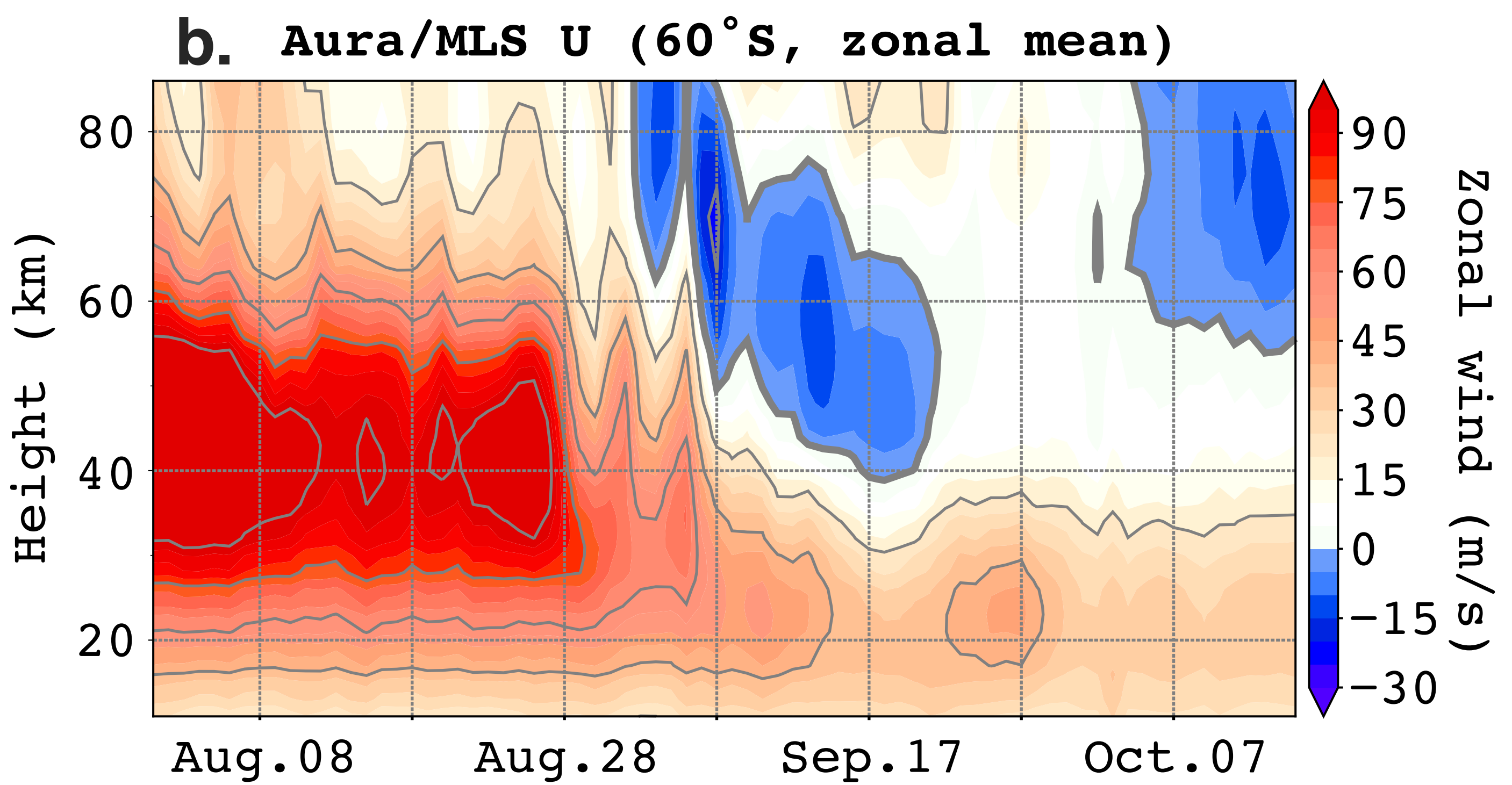
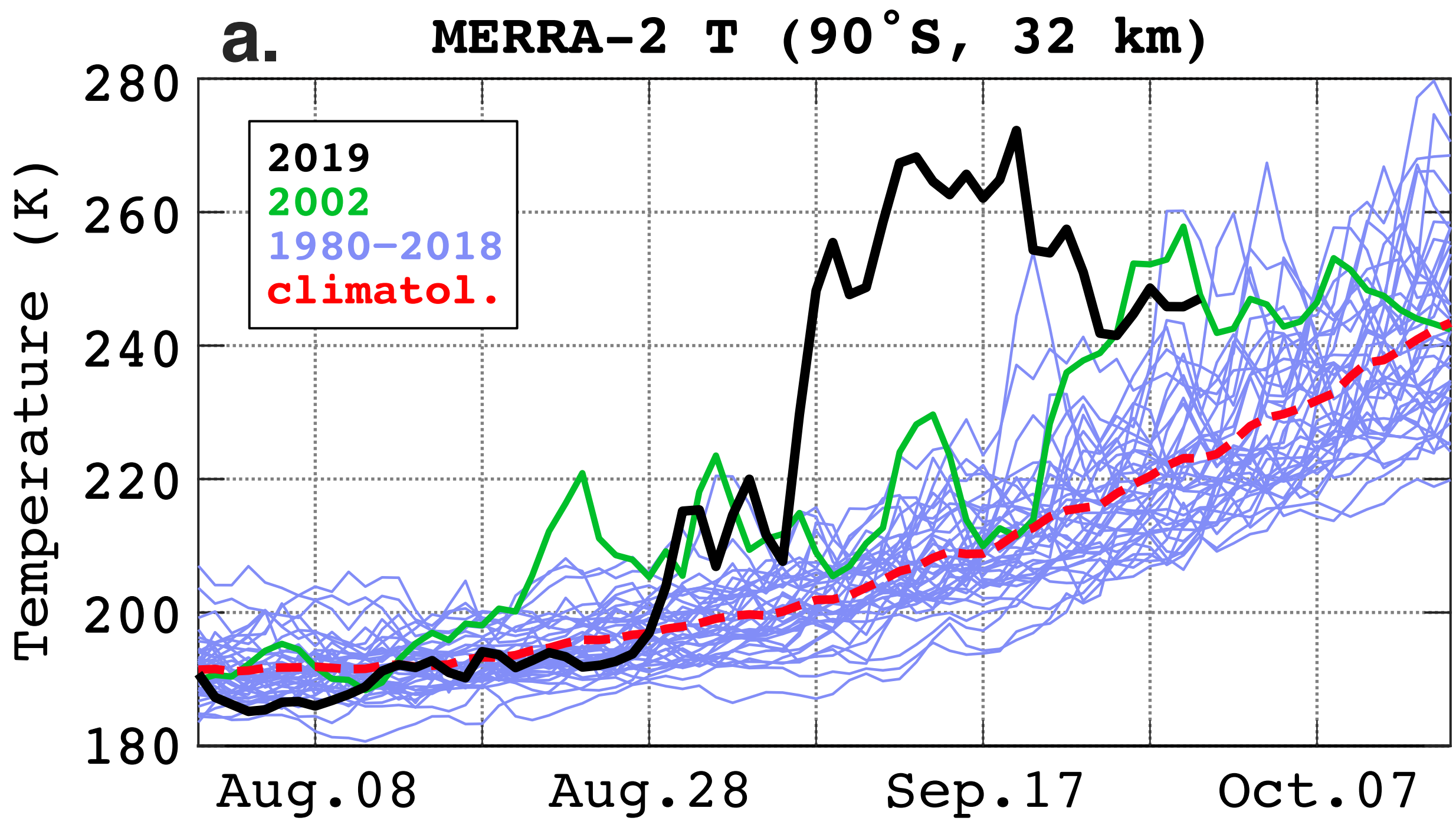


Figure 2.

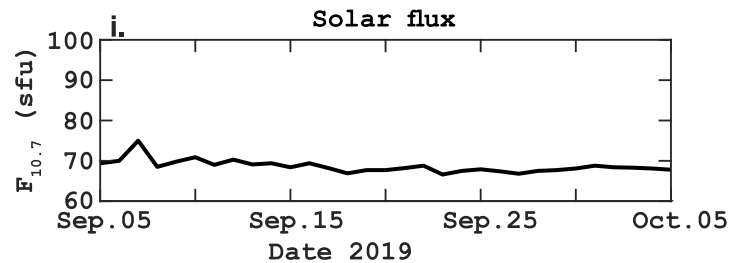
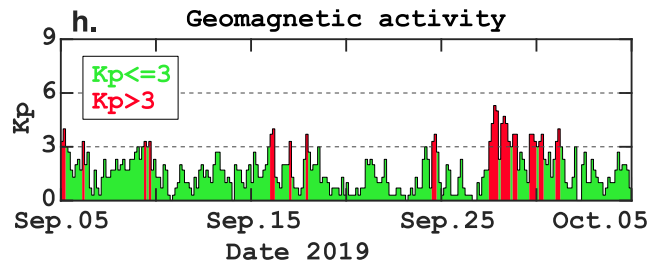
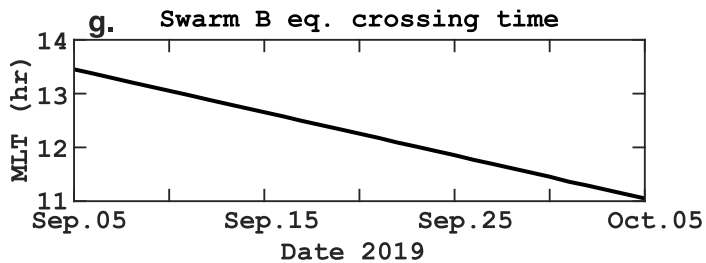
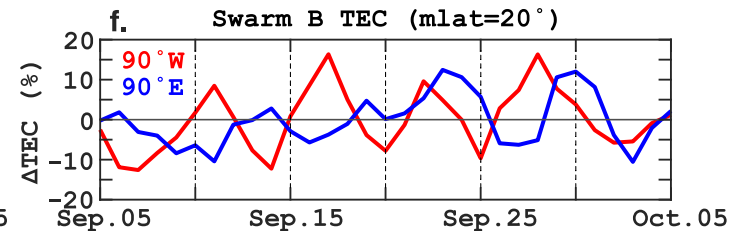
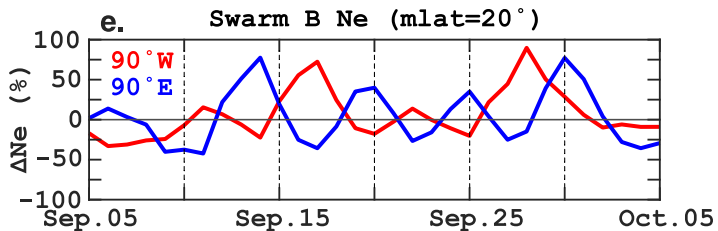
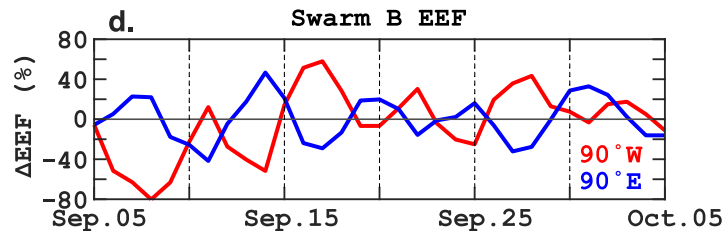
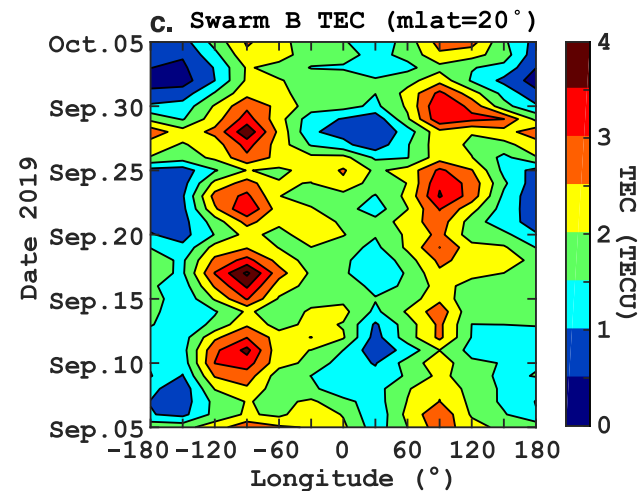
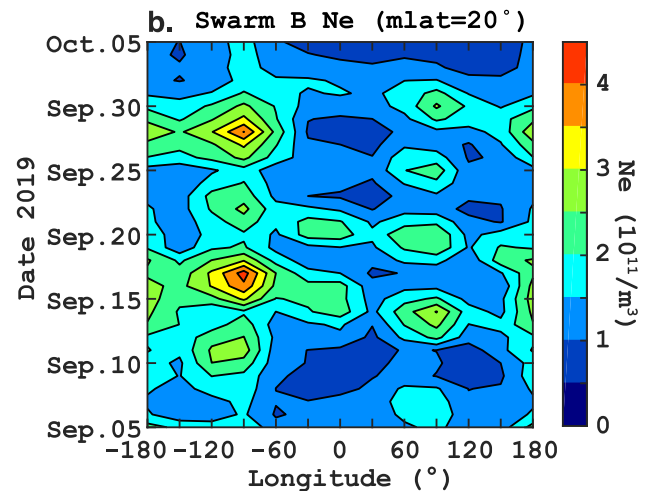
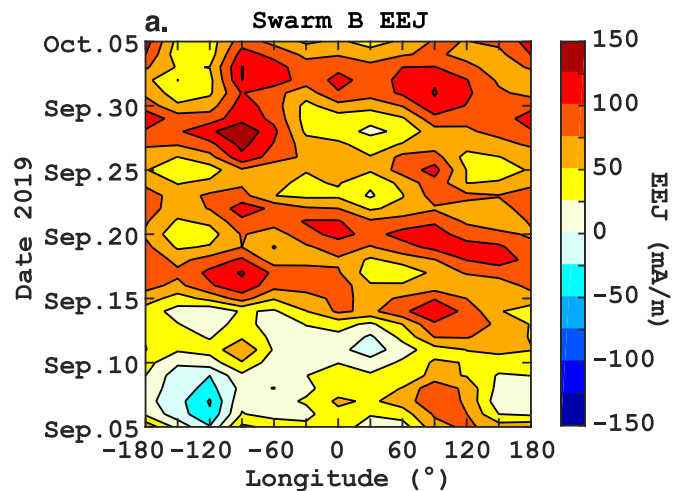


Figure 3.

